J Mol Model (2014) 20:2527
DOI 10.1007/s00894-014-2527-7

ORIGINAL PAPER

Exploring the interactions between isoprenoid chain and labdenediol diphosphate synthase based on molecular docking and quartz crystal microbalance

Wujun Liu · Wei Yang · Yixin Zhang · Zongbao Kent Zhao

Received: 21 June 2014 / Accepted: 10 November 2014 / Published online: 4 December 2014

Abstract Many natural products and biosynthetic intermediates contain isoprenoid chains. Isoprenoid chains are believed to interact with some proteins in the biological systems, but such interactions remain poorly understood. Here labdenediol diphosphate synthase (LPPS) was used as a model to explore the molecular interactions involving isoprenoid chains. Both homology modeling and docking simulation results indicated that binding form between isoprenoid chain and LPPS is dominated by hydrophobic forces in one binding site. The interactions were also examined via quartz crystal microbalance (QCM) technology using synthetic isoprenoid chain-contained probes. The binding constant (1.51 μM^{-1}), binding site number (n=1) and key amino acid residues (Y196, F262, W266, F301, F308, W398, W439, and Y445) were obtained. Both computational and QCM results suggested that LPPS interacts strongly with farnesyl and geranylgeranyl groups. These interactions are primarily caused by hydrophobic and π-π interaction nature. Together, this study provided insightful information to understand molecular interactions between isoprenoid chains and proteins.

Keywords Homology modeling · Isoprenoid chain · Labdenediol diphosphate synthase · Molecular docking · Quartz crystal microbalance

Electronic supplementary material The online version of this article (doi:10.1007/s00894-014-2527-7) contains supplementary material, which is available to authorized users.

W. Liu (✉) · W. Yang · Y. Zhang · Z. K. Zhao
Division of Biotechnology and Dalian National Laboratory for Clean Energy, Dalian Institute of Chemical Physics, CAS, Dalian 116023, People's Republic of China
e-mail: wujunliu@dicp.ac.cn

Introduction

Many natural products or biosynthetic intermediates contain isoprenoid chains, such as isopentenyl, geranyl, farnesyl, and geranylgeranyl groups. Isoprenoid chains are believed to interact with some proteins in the biological systems. However, the molecular interactions, involving isoprenoid chains, remain poorly understood, partially because the moieties are essentially inert in terms of ionic interaction and hydrogen bonding. Nonetheless, it is also recognized that hydrophobic interactions can contribute to ligand-receptor binding [1]. This is particularly important for molecular interactions involving long-chain fatty acids [2]. Recently, we fished out some proteins from the proteome of the yeast *Saccharomyces cerevisiae* by using geranyl containing photoaffinity probes [3]. We further used isoprenoid chain-containing probes and quartz crystal microbalance (QCM) to demonstrate the presence of hydrophobic interactions between isoprenoid chain and some enzymes from *S. cerevisiae* [4]. To attain more insights into molecular interactions involving isoprenoid chains, it will be interesting to examine the structural and interactional aspects of enzymes that are naturally turning over substrate containing isoprenoid chain.

Various terpenoid synthases [5–9] catalyze cyclization reactions of linear isoprenoid precursors, geranyl diphosphate (GPP), farnesyl diphosphate (FPP) or geranylgeranyl diphosphate (GGPP), to give hydrocarbon skeletons of natural drugs, odorants, terpenoids or other metabolic products. Labdenediol diphosphate (LPP) synthase (LPPS) catalyzes the cyclization of GGPP to LPP, which is the key precursor to biosynthesis of amber odorants [10, 11] (Fig. 1). Therefore, the LPPS from *Salvia sclarea*, belonging to terpenoid synthases, can be a potential model for exploring the interaction between protein and isoprenoid chain. Research on the interactions between LPPS and isoprenoid chain should help us to find the protein

binding sites, including residues in substrate hydrophobic transform process, and the regular of isoprenoid diphosphate binding.

In this work, homology modeling and molecular docking were applied to construct a good LPPS model and to investigate its binding information to the isoprenoid moiety and the diphosphate group of isoprenoid diphosphate. QCM and isothermal titration calorimetry (ITC) are important tools for investigating interactions between many biomolecules because of their high sensitivity and the multiplicity of thermodynamic parameters with different protein dosage. Experiments were performed to test interactions between recombinant LPPS and isoprenoid diphosphate derivatives using QCM and ITC techniques. Binding constants, binding site number, key amino acid residues, thermodynamic parameters, and other important binding information were obtained. By analyzing the above data, binding regular, chain length, and the function group effect between isoprenoid diphosphate and LPPS were summarized. The postulated LPPS catalytic mechanism was also briefly discussed.

Materials and methods

Reagents

All chemicals and reagents were purchased from commercial suppliers. Isoprenoid chain-contained chemical probes (**1a**–**1d**) and reference molecules (**2, 3**), sensor chip, enzyme sample, and buffer were prepared as described previously [4]. Farnesyl or geranylgeranyl alcohols (FOH or GGOH) were obtained from Sigma-Aldrich (St. Louis, MO, USA). Geranyl diphosphate (GPP), farnesyl diphosphate (FPP) and geranylgeranyl diphosphate (GGPP) were synthesized according to the literature [12, 13].

Expression and purification of LPPS

PrimeSTAR HS DNA polymerase and restriction enzymes were purchased from TaKaRa (Dalian, China). Oligonucleotides were synthesized by Dingguo Changsheng (Beijing, China). Truncated DNA sequence analysis was performed by TaKaRa. The kits for PCR purification, DNA gel recovery and plasmid miniprep were obtained from Beyotime (Haimen, China). The corresponding truncated LPPS was heterologous overexpressed, purified (Fig. S3), concentrated, and stored in aliquots at −80 °C in elution buffer (pH 8.0) with 10 % glycerol as previous described [14].

Homology modeling

The crystal structure of LPPS is not reported, and constructed by homology modeling using SWISS-MODEL [15], MODELLER (version 9.12) [16], and I–TASSER [17], respectively. The template crystal structures (PDB ID: 3PYA, 3S9V, 3SAE, and 3P5P) and protein sequences were downloaded from the RCSB protein data bank. The bound chemical components and water molecules were removed by AutoDock Tools (ADT), before the crystal structures were used to build the molecular model of LPPS. Procheck, ERRAT, and Profile 3D programs were used to assess homology model accuracy [18–20].

Molecule docking

All ligand structures (Table S1) were built, optimized and saved as .pdbt format using ChemDraw Ultra 8.0 and ADT (version 1.5.4). Docking between ligands and LPPS model was performed using Autodock vina 1.0 [21]. Polar hydrogens were added to ligands and LPPS, and Kollman charges were assigned [22]. A 70×70×70 grid points in the x, y, and z dimensions with 1 Å spacing grid were centered on the reactive residues region. In the docking process, nine conformers were obtained. The conformer with the lowest binding energy was used for docking analysis by Pymol (version 0.99). Chimera (version 1.8) [23], Discovery studio visualizer (version 3.5) [24] and Ligplot^{+} (version 1.4.5) [25] were used to display the protein alignment, structure graphs of homology models and molecular docking results, respectively.

QCM detection

QCM measurement experiments were performed on a 9-MHz AT-cut gold-coated (0.091 cm^2) piezoelectric quartz crystal slab from ANT Technology Co., Ltd. (Taipei, China) at 25 °C. The sensor unit parameters are as follows: flow rate (60 μl/min), resolution (0.1 Hz), sampling period (1 s), temperature range (25±1 °C), voltage (220 V, 50–60 Hz), sample loop volume (100 μl), and cell volume (30 μl). The frequency change (ΔF) was recorded using ADS PLUS (version 8.1; ANT Technology Co., Ltd., China) Software. The kinetic data were analyzed by Affinity Evaluation (version 1.0).

ITC investigation

ITC was performed using a MicroCal™ ITC_{200} (GE Healthcare Bio-Sciences Corp., New Jersey, USA). The titration would not start until the baseline was flat and stable. Titration data were analyzed using Origin (version 7.0) and fitting graph and thermodynamic binding data were obtained in the independent mode. The intrinsic molar enthalpy change (ΔH), binding stoichiometry (n), and binding constant (K_a) for the binding process were obtained from the fit of the calorimetric curve.

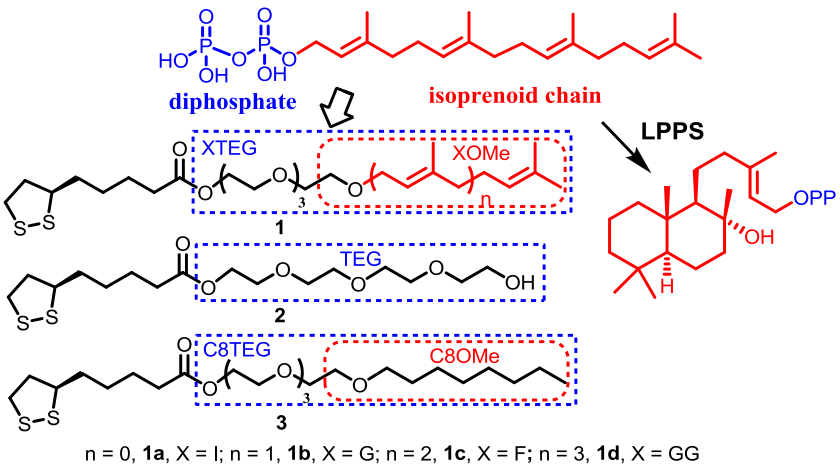

Fig. 1 GGPP cyclization reaction and molecular structure of isoprenoid chain-contained probes (**1a–1d**) and reference molecules (**2**, **3**)

Results and discussion

Homology modeling

The homology modeling was used to generate high resolution hypothetical structure of LPPS by the following evolutionarily related template structure information. The amino acid sequence identity, between LPPS and that of templates (PDB ID: 3PYA, 3S9V, 3SAE, and 3P5P) searched from NCBI protein BLAST, was up to 42 % (ent-copalyl diphosphate synthase, CPPS, PDB ID: 3PYA) [5–8]. Based on the sequence alignment (Fig. 2) and template structure, three protein models were constructed by using SWISS-MODEL, MODELLER, and I–TASSER, respectively.

The models generated by MODELLER were minimized by Chiron [26], while the others were automatically optimized by online server. NIH MBI Laboratory online server was used to assess the quality of the model structures [18]. Based on the online server evaluated results, the best model was constructed by I–TASSER online server. The Ramachandran plot results showed that 99.8 % of the amino acids were in allowed regions, indicating that the accurate model has good stereochemical quality.

Figure 3 showed that 90.5 % of the residues are located in the most favored regions, 7.0 % of the residues in additionally

Fig. 2 Active side protein sequence alignment of LPPS and templates (conserved catalytic residue in *red frame*)

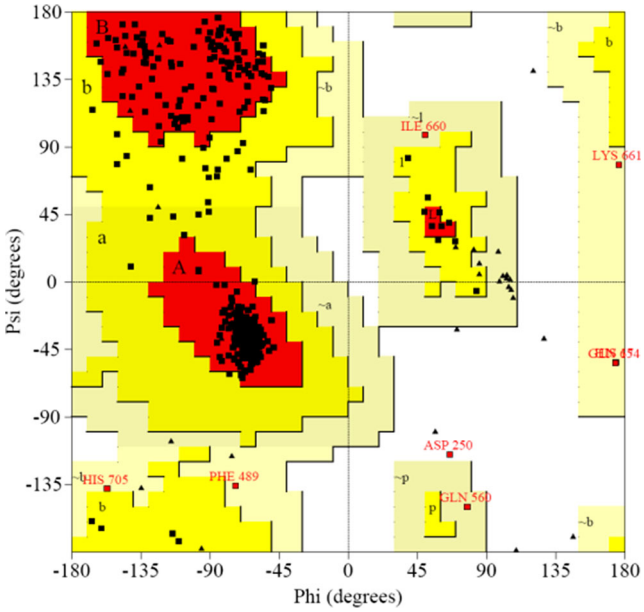

Fig. 3 Ramachandran plot of LPPS model. *Red* most favored regions [*A*, *B*, *L*]; *yellow* additional allowed regions [*a*, *b*, *l*, *p*]; *light yellow* generously allowed regions [*~a*, *~b*, *~l*, *~p*]; other areas disallowed regions

allowed regions and 1.8 % of residues in generously allowed regions. Generally, a qualified model was expected to have over 90 % of residues in the most favored regions [27], this result indicated that the model structure was suitable for further investigation. The structural alignment result between the LPPS model and the crystal structure of CPPS was shown in Fig. 4. The RMSD over all C_α-atoms is 0.83 Å, which illustrated that the model of LPPS was reasonable.

LPPS is composed of 723 amino acids containing a DXDD motif and belongs to class II cyclase of terpenoid cyclases [8]. It contains three structurally different α-helices domains, α (Ser45–His255), β (Met1–Ile44, Thr256–Phe463), and γ (Asn464–Val723) (Fig. 4). Domains α, β and domains β, γ are linked by the stretched loops and α–helix, respectively. However, LPPS lacks metal binding motifs in the α domain, consistent with the lack of ionization-dependent class I cyclase activity [28].

Molecular docking

Docking is a method of predicting the most favorable binding mode between LPPS and GGPP toward forming a stable complex. Orientation of probe moiety in LPPS active site played a major role in determining their association strength (binding affinity). According to the structure information of CPPS, CPPS and LPPS may bind the same substrate and have similar structural product. The active site of LPPS resides in a deep cavity at the αβ interface and is more open and solvent-accessible. To investigate the interaction between isoprenoid chain and LPPS, we docked LPPS with GGPP, FPP, GPP, IPP, and the fragments of compounds **1**, **2**, and **3** (Table S1).

Interestingly, the fragments of isoprenoid-containing probe and LPPS docking results (Fig. 5) showed that GGOMe (8.4 kcal mol^{-1}) and GGPP (8.1 kcal mol^{-1}) have almost the same affinity energy, and that of GGTEG is 7.2 kcal mol^{-1}. Tetraethylene glycol (TEG) group increased the binding energy because the larger GGTEG fragment and GGPP might share the same binding residues of LPPS cavity (Fig. S2). Generally, hydrophobic interactions are much weaker than ionic and hydrogen bond interaction. However, the docking results indicated that hydrophobic interaction can play a leading role in the event that there are two or more isoprenoid units in substrate. Another structural characteristic that could not be neglected was the isoprenoid chain carbon-carbon double bond, which could provide π-π interaction. Docking data showed that the binding between GGPP, FPP, GPP, and LPPS was dominated by π-π interaction and hydrophobic force.

The best GGPP and LPPS docking complex, in which residues within 6 Å were selected around the ligand, was shown in Fig. 6. The linear GGPP binds LPPS that the isoprenoid tail extends toward the end of the active site, and the diphosphate group binds the residues (A140, G141, N193, Q349, V351, and R397) at the mouth of the active site. The hydrophobic, numerous aliphatic and aromatic residues of LPPS active site cavity (Fig. 7) is the interaction structural basis between isoprenoid chain and LPPS.

According to Fig. 7, there are hydrogen bond interactions between diphosphate of GGPP and the residue G141 and R397, and the lengths of the hydrogen bonds are 3.0 and

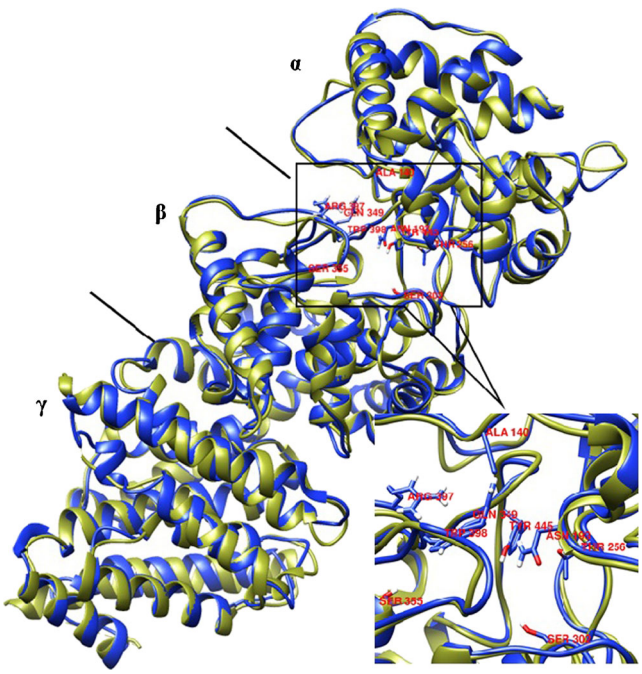

Fig. 4 Superposition models of LPPS (*blue*) and crystal structure of ent-copalyl diphosphate synthase (*drab*)

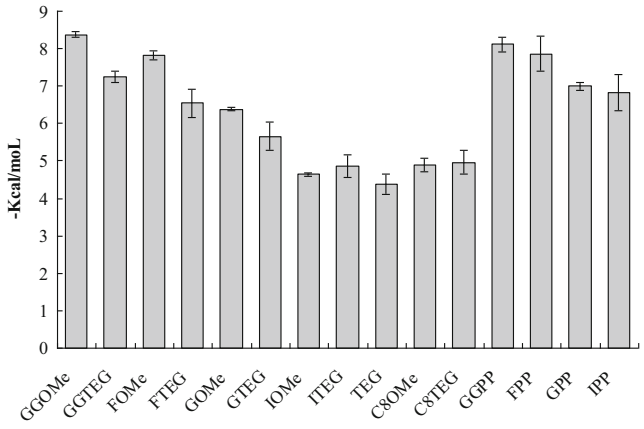

Fig. 5 Docking results of isoprenoid diphosphate and isoprenoid containing fragment of probes

2.8 Å, respectively. Hydrogen bond might help GGPP find the entrance of cavity, bind with LPPS, and extend its tail toward the end of the active cavity [29]. The aromatic side chains, Y196, F262, W266, F301, F308, W398, W439, and Y445, could bind isoprenoid substrate and stabilize carbocation intermediate in GGPP cyclic process via cation-π interactions.

Class II cyclases contain a DXDD acidic motif, in which the D312 may catalyze the ensuing multi-step cyclization cascade. In the traditional mechanism [30, 31], magnesium ion must be

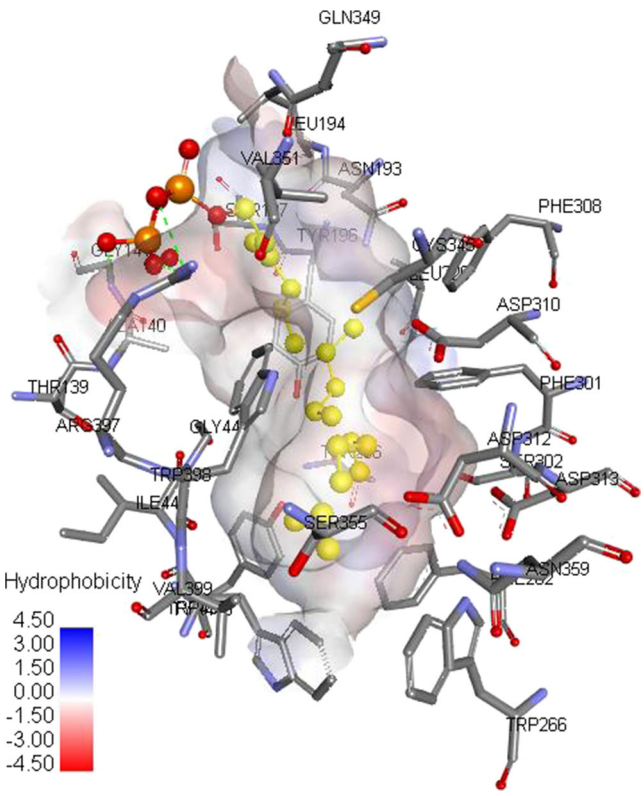

Fig. 6 Docking complex of GGPP in LPPS amphiprotic cavity. The residues of LPPS were represented using stick and GGPP was represented using a scaled ball and stick model. The hydrogen bonds between GGPP and the LPPS were represented using *green dashed lines*

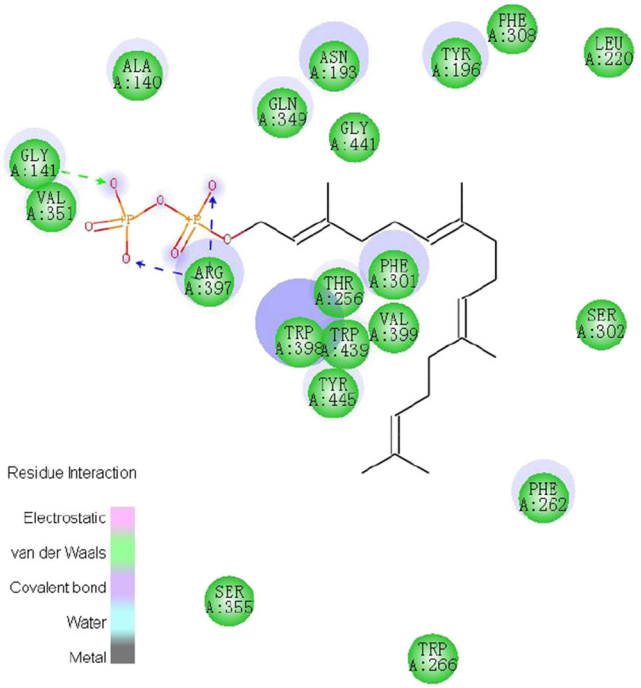

Fig. 7 Two-dimensional representation for interaction mode of GGPP with LPPS

involved to activate the water molecule to finish the hydroxylation reaction of the carbocation intermediate. However, we proposed the key catalytic step of LPPS is different from that of traditional mechanism. With the help of S355 and N359, the proposed carbocation intermediate, stabilized by W398, is ultimately terminated by concerted water proton elimination and hydroxyl capture. This mechanism could be indirectly supported by the following ITC analysis.

Protein expression and purification

The DNA sequence of LPPS in *Salvia sclarea* was optimized for codon preference [10]. To achieve protein over expression, we truncated the excess signal peptide (Fig. S1) and cloned it into pET24b vector generating pET24b-tLPPS. The resulting expression vector pET24b-tLPPS was transformed into *E. coli* BL21 (DE3). As the SDS-PAGE (Fig. S3) showed, the molecule weight of LPPS is approximately 82 kDa.

QCM and ITC experiments

In QCM analysis, the ΔF value is determined by the Sauerbrey's equation [32]:

$$\Delta F = -F_0^{3/2}\left(\frac{\rho_1\eta_1}{\pi\rho_q\mu_q}\right)^{1/2}$$

where ΔF is the frequency shift, F_0 is the intrinsic resonant frequency of the crystal, ρ_l and η_l respectively are the density

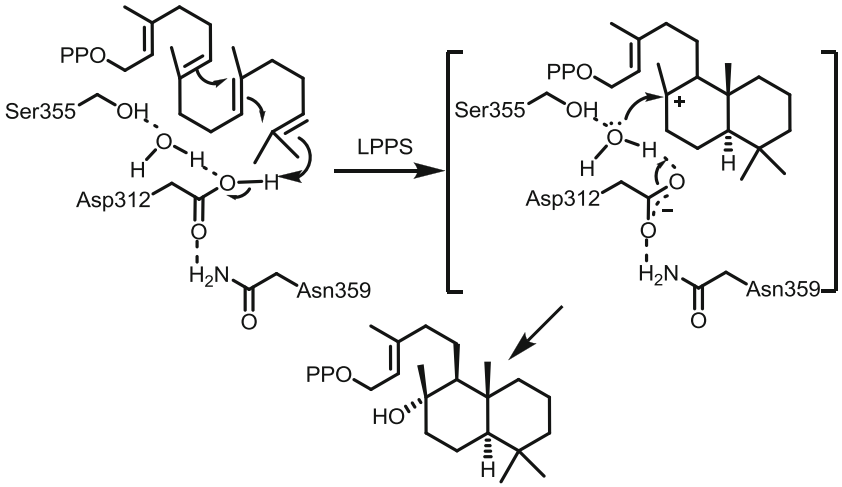

Fig. 8 Postulated mechanism of cyclic reaction catalyzed by Ser355, Asp312, and Asn359

and viscosity of the liquid in contact with the crystal, ρ_q is the density of quartz (2.648 g cm^{-3}) and μ_q is the shear modulus of quartz (2.947×10^{11} g cm^{-1} s^{-2}). One Hertz frequency change corresponds to 0.55 ng mass change according to ANT Corporation supporting information.

Frequency shifts were maximum when the molar ratio between **1** and **2** was 2:1 on QCM chip as previously described [4]. The frequency shifts induced by LPPS for those chips modified by **1a**–**1d** indicated the different molecular interactions between LPPS and **1a**–**1d**. Gradually larger frequency shifts were found from **1a** to **1d**, and only the frequency shift for **1a** was smaller than that of reference molecule **3** (Fig. 9), in which octanyl group was presented in lieu of isoprenoid group. These results suggested that interactions between isoprenoid chain and LPPS increased in proportion to the length of isoprenoid chain. The **3**-LPPS shift change was a little higher than that of **1a**, but much lower than that of **1b** which indicated that π-π interaction played an important role besides hydrophobic interaction.

To investigate the detailed regularity of the strongest interaction pair, **1d** and LPPS, kinetic experiment for binding affinity parameters was processed. The Scatchard plot (Fig. 10) showed that the association constant (K_a) and the molecular binding number (n) for **1d** binding to LPPS were determined as 1.51 μM^{-1} and 1.05, respectively. The docking association constant (K_a=5 μM^{-1}) was approximately five times than that of QCM according to the Gibbs equation:

$$\Delta G = -RT\ln K_d$$

where K_d ($1/K_a$) is the dissociation constant and the docking energy (ΔG) between GGTEG and LPPS is −7.2 kcal mol^{-1} R and T present the molar gas constant (8.314 J $(mol\ K)^{-1}$) and temperature (298 K). The different results might be due to the QCM on-chip ligand-receptor interaction form is different from the free ligand-receptor binding mode in solution. LPPS has one active site, which is consistent with that of class II cyclases, to interact with **1d** [28]. Both molecule docking and QCM results demonstrated that isoprenoid chain, instead of diphosphate group, made the main contribution to isoprenoid diphosphate and LPPS binding.

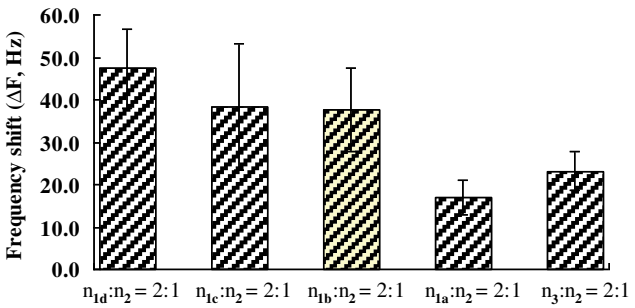

Fig. 9 QCM analysis of molecular interactions between synthetic probes **1a**–**1d** and LPPS. (The maximum saturation binding concentration of LPPS was 110 μg ml^{-1})

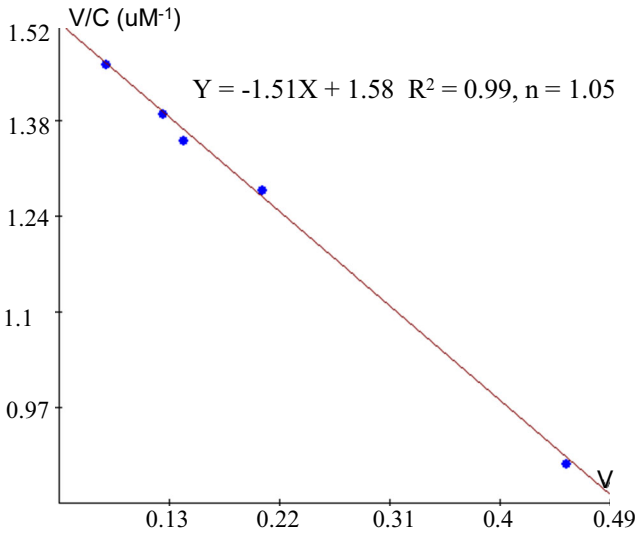

Fig. 10 Scatchard plot of GGTEG binding affinity to LPPS. The quartz chip was modified by a mixture of **1d** and **2** in a molar ratio of 2:1. (*V*: $\Delta F/\Delta F_{max}$, *C*: concentration of LPPS)

In addition, isothermal titration calorimetry (ITC) was also used to characterize the thermodynamics of LPPS and ligands. We tried GPP, FPP, GGPP, FTEG, and GGTEG probe and other molecule segments, but the solubility of these compounds in MOPS buffer is too small for ITC interaction detection. Thus, DMSO, as a co-solvent, was added to dissolve ligands. Although 50 % of DMSO could help dissolve FPP, GGPP, FTEG, GGTEG, and other hydrophobic ligands, high DMSO concentration was not permitted for ITC detection for the mixing thermal effect and LPPS stability. Although the bonding constant for **1d** and LPPS was not determined, we investigated the interaction between LPPS and GPP, which had better solubility than GGPP and FPP in MOPS buffer containing 20 % DMSO. Interestingly, large enthalpy changes were observed without magnesium ion added in MOPS buffer and the reaction achieved equilibrium in no time (data not shown). This result indicated that the high activity of truncated LPPS, which was over-expressed in *E. coli*, could catalyze substrate cyclization using DXDD domain without magnesium ion. We could postulate that the mechanism was different from the traditional mechanism [30, 31], in which another water molecule was activated by magnesium ion. In this process of cyclization, one water molecule's proton elimination and hydroxyl capture was an ensuing multi-step cyclization cascade without magnesium ion activation. Thus, the ITC results also might indirectly support the postulated reaction mechanism in Fig. 8. After we optimized the parameters and experimental condition, the calculated Gibbs free energy average was below zero. It is indicated that the geranyl chain and LPPS binding and cyclization were a spontaneous process.

Conclusions

The interactions between isoprenoid diphosphate and LPPS were investigated by combining computational simulation and electro and thermo chemistry analysis. From the docking results and frequency shifts of QCM, the strong molecular interactions were found to occur in LPPS-isoprenoid chain pairs. When isoprenoid unit number was greater than two, π-π interaction and hydrophobic force played a principal function over that of diphosphate group hydrogen and ionic bond. These results suggested that π-π interaction and hydrophobic force of isoprenoid chain were the main binding basis for natural terpenoid synthase with the isoprenoid diphosphate molecule. The aromatic amino acid residues of LPPS hydrophobic cavity could help isoprenoid chain unit binding and stabilize the cyclic carbocation intermediate from the docking analysis. The Gibbs free energy of docking and ITC results showed that isoprenoid diphosphate and LPPS binding and substrate cyclization catalyzed by DXDD was a spontaneous process. According to Scatch plot of QCM, the binding constant (K_a) and binding number (n) between the donor (isoprenoid chain units) and the acceptor (LPPS) were proved to be consistent with the docking results. This study, by combining modeling and docking with QCM and ITC, provided a rational basis for investigating and fundamental understanding of non-hydrogen bond interactions between isoprenoid chain units and their receptors in biological systems.

Acknowledgments We are grateful for the support of the National Natural Science Foundation of China (No. 20972158, 21102143).

References

1. Toth G, Bowers SG, Truong AP, Probst G (2007) The role and significance of unconventional hydrogen bonds in small molecule recognition by biological receptors of pharmaceutical relevance. Curr Pharm Des 13(34):3476–3493. doi:10.2174/138161207782794284
2. Tan MC, Matsuoka S, Ano H, Ishida H, Hirose M, Sato F, Sugiyama S, Murata M (2014) Interaction kinetics of liposome-incorporated unsaturated fatty acids with fatty acid-binding protein 3 by surface plasmon resonance. Bioorg Med Chem. doi:10.1016/j.bmc.2014.02.001
3. Tian R, Li L, Tang W, Liu H, Ye M, Zhao ZK, Zou H (2008) Chemical proteomic study of isoprenoid chain interactome with a synthetic photoaffinity probe. Proteomics 8(15):3094–3104. doi:10.1002/pmic.200800021
4. Liu W, Zhang Y, Hou S, Zhao ZK (2013) Synthesis of isoprenoid chain-contained chemical probes for an investigation of molecular interactions by using quartz crystal microbalance. Tetrahedron Lett 54(46):6208–6210. doi:10.1016/j.tetlet.2013.09.004
5. Köksal M, Jin Y, Coates RM, Croteau R, Christianson DW (2010) Taxadiene synthase structure and evolution of modular architecture in terpene biosynthesis. Nature 469(7328):116–120. doi:10.1038/nature09628
6. Zhou K, Gao Y, Hoy JA, Mann FM, Honzatko RB, Peters RJ (2012) Insights into diterpene cyclization from structure of bifunctional abietadiene synthase from abies grandis. J Biol Chem 287(9):6840–6850. doi:10.1074/jbc.M111.337592
7. McAndrew RP, Peralta-Yahya PP, DeGiovanni A, Pereira JH, Hadi MZ, Keasling JD, Adams PD (2011) Structure of a three-domain sesquiterpene synthase: a prospective target for advanced biofuels production. Structure 19(12):1876–1884. doi:10.1016/j.str.2011.09.013
8. Koksal M, Hu H, Coates RM, Peters RJ, Christianson DW (2011) Structure and mechanism of the diterpene cyclase ent-copalyl diphosphate synthase. Nat Chem Biol 7(7):431–433. doi:10.1038/nchembio.578
9. Paddon CJ, Westfall PJ, Pitera DJ, Benjamin K, Fisher K, McPhee D, Leavell MD, Tai A, Main A, Eng D, Polichuk DR, Teoh KH, Reed DW, Treynor T, Lenihan J, Fleck M, Bajad S, Dang G, Diola D, Dorin G, Ellens KW, Fickes S, Galazzo J, Gaucher SP, Geistlinger T, Henry R, Hepp M, Horning T, Iqbal T, Jiang H, Kizer L, Lieu B, Melis D, Moss N, Regentin R, Secrest S, Tsuruta H, Vazquez R, Westblade LF, Xu L, Yu M, Zhang Y, Zhao L, Lievense J, Covello PS, Keasling JD, Reiling KK, Renninger NS, Newman JD (2013) High-level semi-synthetic production of the potent antimalarial artemisinin. Nature 496:528–532. doi:10.1038/nature12051
10. Yang W, Zhou Y, Liu W, Shen H, Zhao ZK (2013) Engineering Saccharomyces cerevisiae for sclareol production. Chin J Biotechnol 29(8):1185–1192

11. Aricò F, Tundo P, Maranzana A, Tonachini G (2012) Synthesis of five-membered cyclic ethers by reaction of 1,4-diols with dimethyl carbonate. ChemSusChem 5(8):1578–1586. doi:10.1002/cssc.201100755
12. Zhang H, Shibuya K, Hemmi H, Nishino T, Prestwich GD (2006) Total synthesis of geranylgeranylglyceryl phosphate enantiomers: substrates for characterization of 2,3-o-digeranylgeranylglyceryl phosphate synthase. Org Lett 8(5):943–946. doi:10.1021/ol0530878
13. Thulasiram HV, Phan RM, Rivera SB, Poulter CD (2006) Synthesis of deuterium-labeled derivatives of dimethylallyl diphosphate. J Org Chem 71(4):1739–1741. doi:10.1021/jo052384n
14. Wang J, Tan H, Zhao Z (2007) Over-expression, purification, and characterization of recombinant NAD-malic enzyme from Escherichia coli K12. Protein Expr Purif 53(1):97–103. doi:10.1016/j.pep.2006.11.017
15. Biasini M, Bienert S, Waterhouse A, Arnold K, Studer G, Schmidt T, Kiefer F, Cassarino TG, Bertoni M, Bordoli L, Schwede T (2014) SWISS-MODEL: modelling protein tertiary and quaternary structure using evolutionary information. Nucleic Acids Res. doi:10.1093/nar/gku340
16. Eswar N, Webb B, Marti-Renom MA, Madhusudhan M, Eramian D, Shen M-y, Pieper U, Sali A (2006) Comparative protein structure modeling using Modeller. Current protocols in bioinformatics, vol Supplement 15. Wiley, New York
17. Roy A, Kucukural A, Zhang Y (2010) I-TASSER: a unified platform for automated protein structure and function prediction. Nat Protoc 5(4):725–738. doi:10.1038/nprot.2010.5
18. Laskowski RA, MacArthur MW, Moss DS, Thornton JM (1993) PROCHECK: a program to check the stereochemical quality of protein structures. J Appl Crystallogr 26:283–291. doi:10.1107/S0021889892009944
19. Colovos C, Yeates TO (1993) Verification of protein structures: patterns of nonbonded atomic interactions. Protein Sci 2(9):1511–1519. doi:10.1002/pro.5560020916
20. Bowie JU, Luthy R, Eisenberg D (1991) A method to identify protein sequences that fold into a known three-dimensional structure. Science 253(5016):164–170. doi:10.1126/science.1853201
21. Trott O, Olson AJ (2010) AutoDock Vina: improving the speed and accuracy of docking with a new scoring function, efficient optimization and multithreading. J Comput Chem 31:455–461. doi:10.1002/jcc.21334
22. Gasteiger J, Marsili M (1980) Iterative partial equalization of orbital electronegativity—a rapid access to atomic charges. Tetrahedron 36(22):3219–3228. doi:10.1016/0040-4020(80)80168-2
23. Pettersen EF, Goddard TD, Huang CC, Couch GS, Greenblatt DM, Meng EC, Ferrin TE (2004) UCSF Chimera—a visualization system for exploratory research and analysis. J Comput Chem 25(13):1605–1612. doi:10.1002/jcc.20084
24. Discovery Studio Visualizer 3.5 (2013) Accelrys Inc, San Diego
25. Laskowski RA, Swindells MB (2011) LigPlot+: multiple ligand–protein interaction diagrams for drug discovery. J Chem Inf Model 51(10):2778–2786. doi:10.1021/ci200227u
26. Ramachandran S, Kota P, Ding F, Dokholyan NV (2011) Automated minimization of steric clashes in protein structures. Proteins Struct Funct Bioinforma 79(1):261–270. doi:10.1002/prot.22879
27. Patel A, Dewangan R, Khatri S, Choubey J, Gupta SK, Verma M (2009) Identification of insilico 3D structure of amylase (Drosophila melanogaster) and comparative computational studies. J Eng Technol Res 1(2):039–045
28. Prisic S, Xu J, Coates RM, Peters RJ (2007) Probing the role of the DXDD motif in class II diterpene cyclases. ChemBioChem 8(8):869–874. doi:10.1002/cbic.200700045
29. Turek-Etienne T, Strickland C, Distefano M (2003) Biochemical and structural studies with prenyl diphosphate analogues provide insights into isoprenoid recognition by protein farnesyl transferase. Biochemistry 42(13):3716–3724. doi:10.1021/bi0266838
30. Schalk M, Pastore L, Mirata MA, Khim S, Schouwey M, Deguerry F, Pineda V, Rocci L, Daviet L (2012) Toward a biosynthetic route to sclareol and amber odorants. J Am Chem Soc 134(46):18900–18903. doi:10.1021/ja307404u
31. Potter K, Criswell J, Zi J, Stubbs A, Peters RJ (2014) Novel product chemistry from mechanistic analysis of ent-copalyl diphosphate synthases from plant hormone biosynthesis. Angew Chem Int Ed. doi:10.1002/anie.201402911
32. Dunham GC, Benson NH, Petelenz D, Janata J (1995) Dual quartz crystal microbalance. Anal Chem 67(2):267–272. doi:10.1021/ac00098a005